RESEARCH ARTICLE

Figures and figure supplements

Multivalency, autoinhibition, and protein disorder in the regulation of interactions of dynein intermediate chain with dynactin and the nuclear distribution protein

Kayla A Jara *et al*.

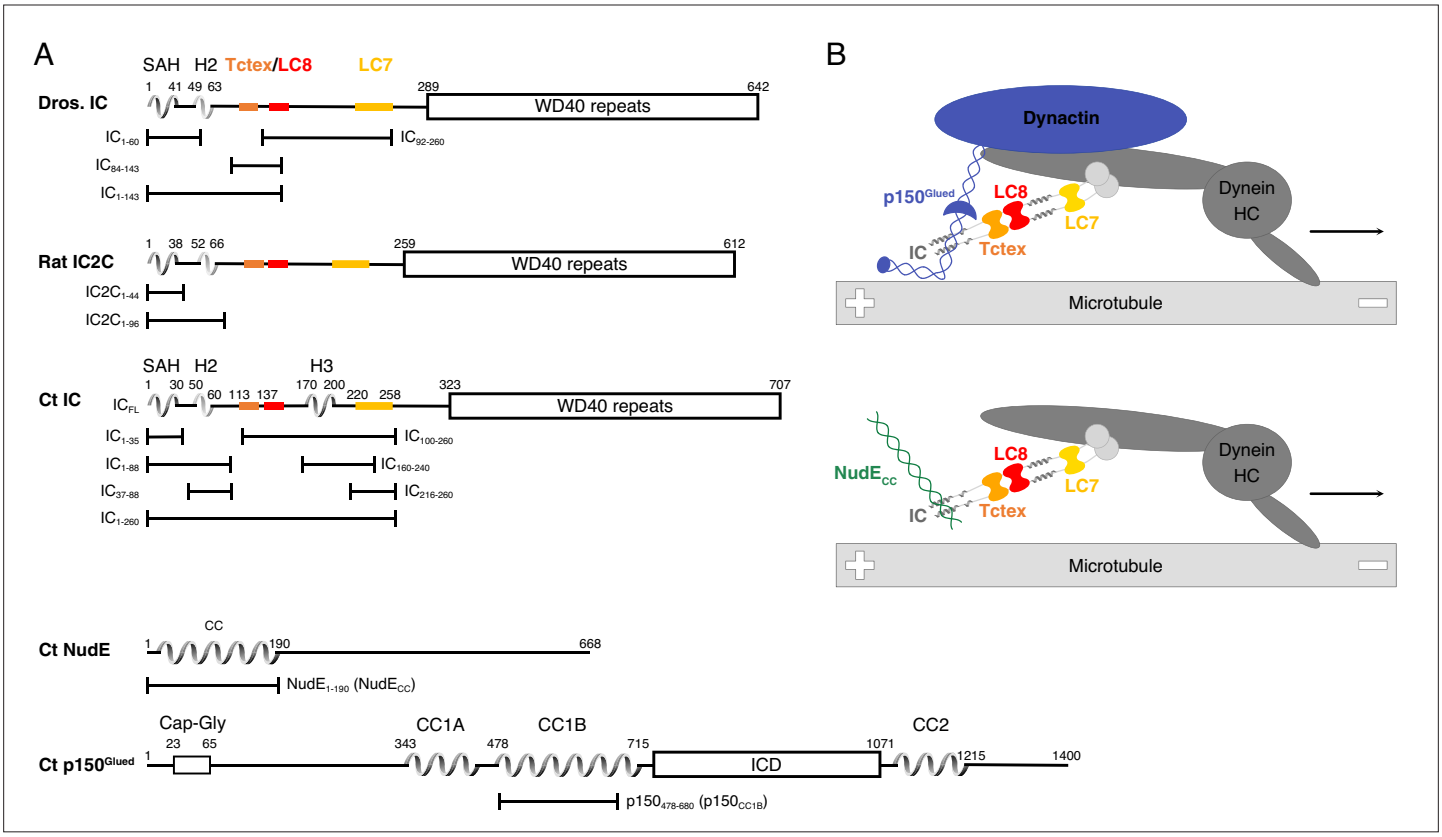

Figure 1. Domain architecture for dynein intermediate chain (IC), dynactin p150^{Glued}, and nuclear distribution protein (NudE). (**A**) Domain architecture diagrams for IC from *Drosophila melanogaster* (Dros. IC) and *Rattus norvegicus* (Rat IC2C) and constructs used in earlier work are provided for comparison. Proteins and constructs used in this work are from *Chaetomium thermophilum* (Ct). All ICs have an N-terminal single α-helix (SAH), followed by either a transient/nascent or folded second helix (H2). In Ct, there is an additional helix (H3). The Tctex (orange), LC8 (red), and LC7 (yellow) binding sites are well characterized in Dros. IC and Rat IC2C, and their position in Ct were predicted based on sequence and structure comparison. The C-terminal domain is predicted to contain seven WD40 repeats. The Ct constructs IC_{FL}, $IC_{1\text{-}88}$, $IC_{37\text{-}88}$, $IC_{1\text{-}260}$, $IC_{100\text{-}260}$, $IC_{140\text{-}260}$, $IC_{216\text{-}260}$, and $IC_{216\text{-}260}$ are used in this paper; the $IC_{1\text{-}35}$ construct was used in prior work. Ct p150^{Glued} is predicted to have a Cap-Gly domain near the N-terminus, and two coiled-coil (CC) domains, CC1 and CC2, that are separated by an intercoil domain. CC1 is further divided into two regions called CC1A and CC1B. $p150_{478\text{-}680}$ ($p150_{CC1B}$) is the construct used in this work. Ct NudE is predicted to have an N-terminal CC region followed by disorder. $NudE_{1\text{-}190}$ ($NudE_{CC}$) is the construct used in this work. (**B**) Contextual models of dynein with the heavy chains (HC) crudely shown in dark gray. IC in the subcomplex (light gray) is shown in the same orientation as the domain architecture schematic in panel A. The top model depicts the interaction between the p150^{Glued} subunit of dynactin (blue) and the SAH and H2 regions of IC while the bottom model depicts the interaction between $NudE_{CC}$ (green) and the SAH region of IC. In both models, dynein is a processive motor traveling toward the minus end of a microtubule, and IC is shown with the homodimeric dynein light chains: Tctex (orange), LC8 (red), and LC7 (yellow).

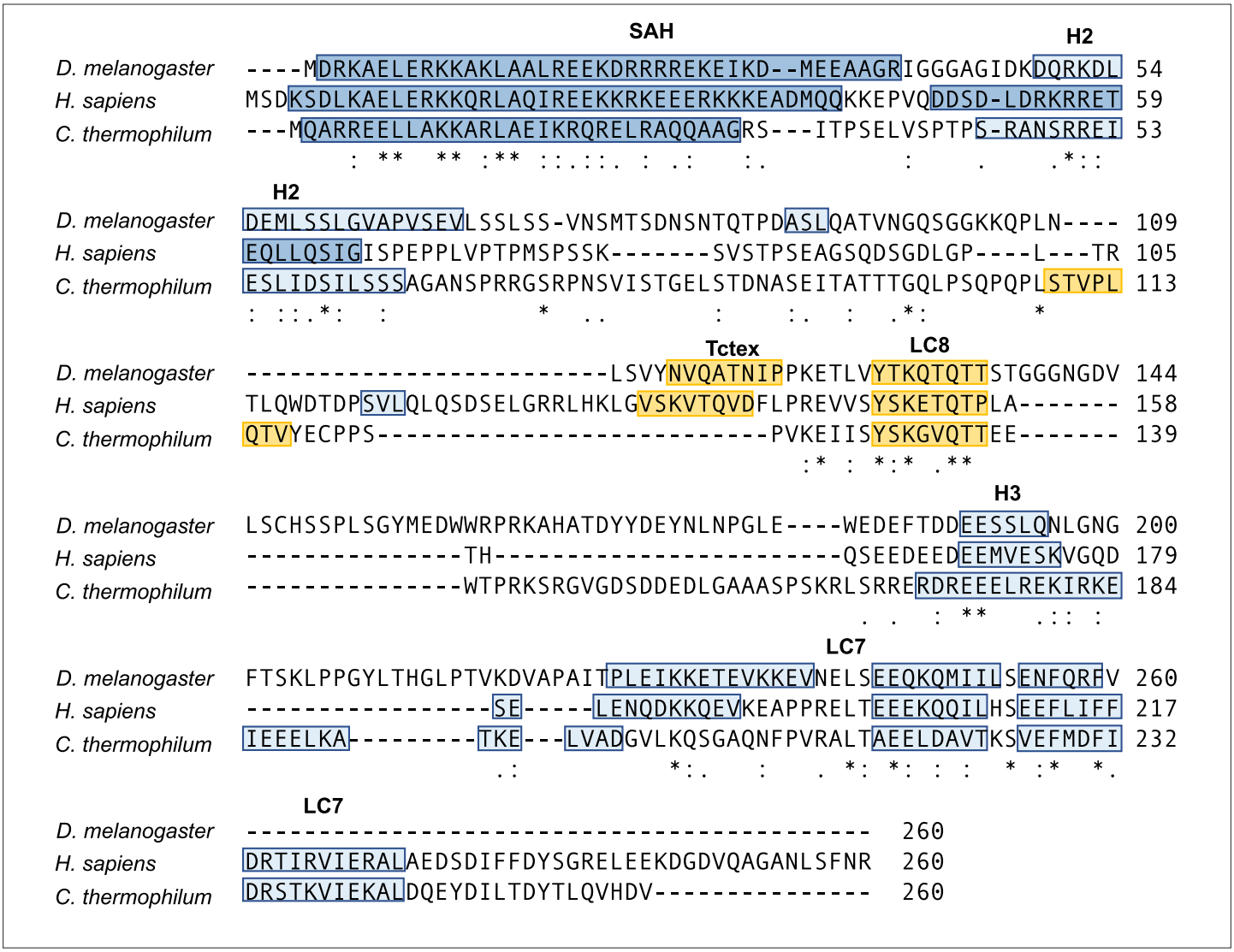

Figure 1—figure supplement 1. Intermediate chain (IC) sequence alignment. Alignment of the first 260 residues of IC from *Drosophila*, human, and *Chaetomium thermophilum* using the Multiple Alignment using Fast Fourier Transform (MAFFT) alignment program (***Katoh and Standley, 2013***). Identical (asterisk), strongly similar (colon), and weakly similar (period) residues are shown at the bottom of each alignment. Known or predicted α-helical secondary structure (single α-helix [SAH], H2, H3, and the LC7 binding domain) is highlighted in blue, with the darker shade of blue indicating stronger prediction. Known or predicted binding sites for Tctex and LC8 are highlighted in yellow (***Jespersen et al., 2019***).

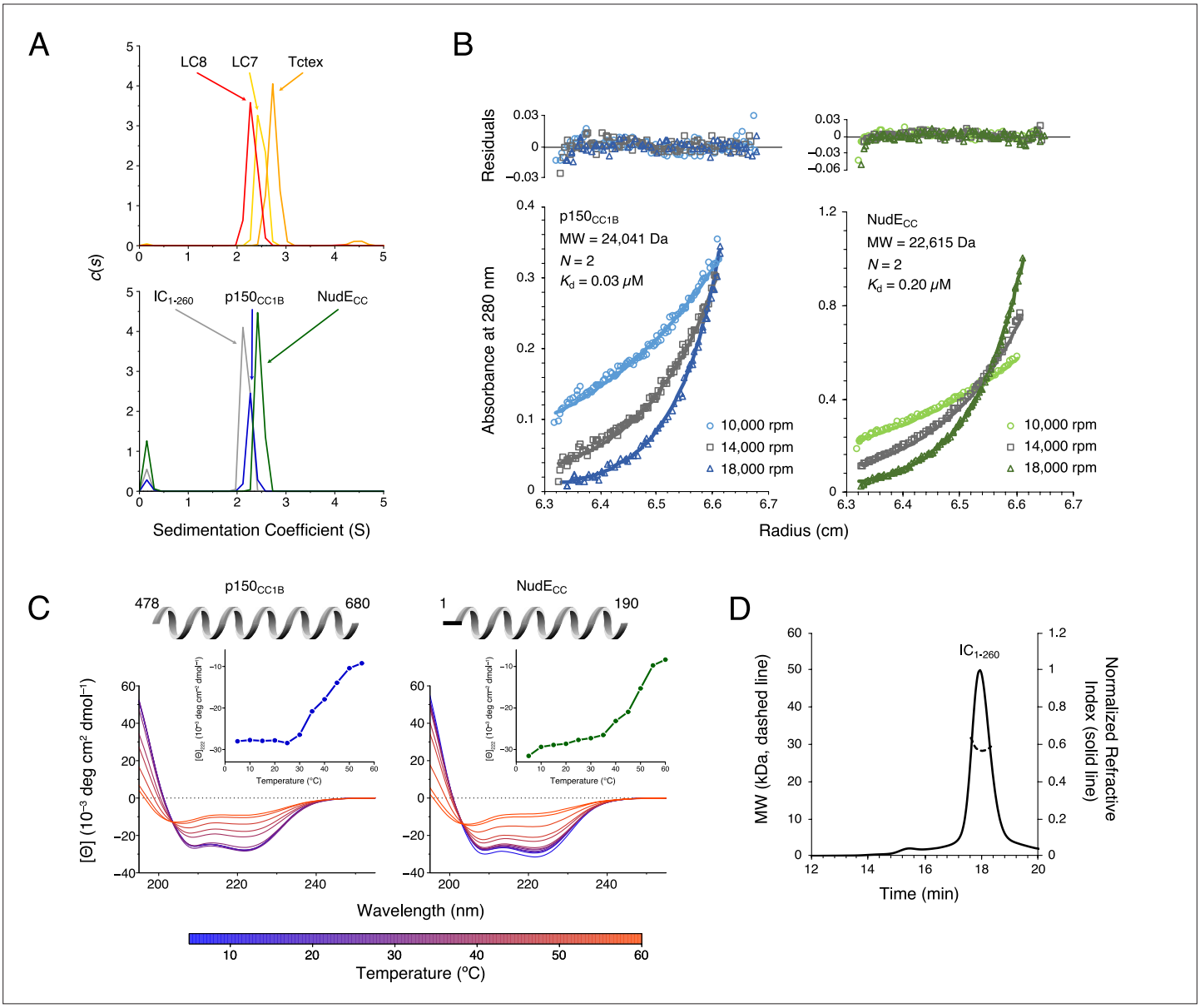

Figure 2. *Chaetomium thermophilum* (Ct) $p150_{CC1B}$, $NudE_{CC}$, and dynein light chains are dimeric, whereas Ct $IC_{1\text{-}260}$ is monomeric. (**A**) Sedimentation velocity analytical ultracentrifugation profiles for LC8 (red), LC7 (yellow), and Tctex (orange) (top), and, $IC_{1\text{-}260}$ (gray), $p150_{CC1B}$ (blue), and $NudE_{CC}$ (green) (bottom). All samples were at protein concentration of 30 μM. (**B**) Sedimentation equilibrium analytical ultracentrifugation data for $p150_{CC1B}$ (blue) and $NudE_{CC}$ (green) at three speeds (10,000, 14,000, and 18,000 rpm). Data were fit to a monomer-dimer binding model. The quality of the fits to this model is reflected by the plots of the residuals on top. The monomeric masses determined by fitting this data compare very well to the masses expected based on the sequences for the constructs. The stoichiometry (*N*) values of 2 indicate that both $p150_{CC1B}$ and $NudE_{CC}$ are dimers in solution. (**C**) Circular dichroism spectra of $p150_{CC1B}$ and $NudE_{CC}$ acquired at temperatures in the 5–60°C range. The shape of the spectra for both $p150_{CC1B}$ and $NudE_{CC}$ indicates α-helical secondary structure, and the 222/208 ratios (1.04 and 1.00 for $p150_{CC1B}$ and $NudE_{CC}$, respectively) are consistent with coil-coiled structures. Inset graphs show the molar ellipticity at 222 nm as a function of temperature. (**D**) Multi-angle light scattering of $IC_{1\text{-}260}$ gives an estimated mass of 29.5 kDa, which indicates that, on its own, $IC_{1\text{-}260}$ exists as a monomer in solution (calculated mass of monomer is 29.2 kDa).

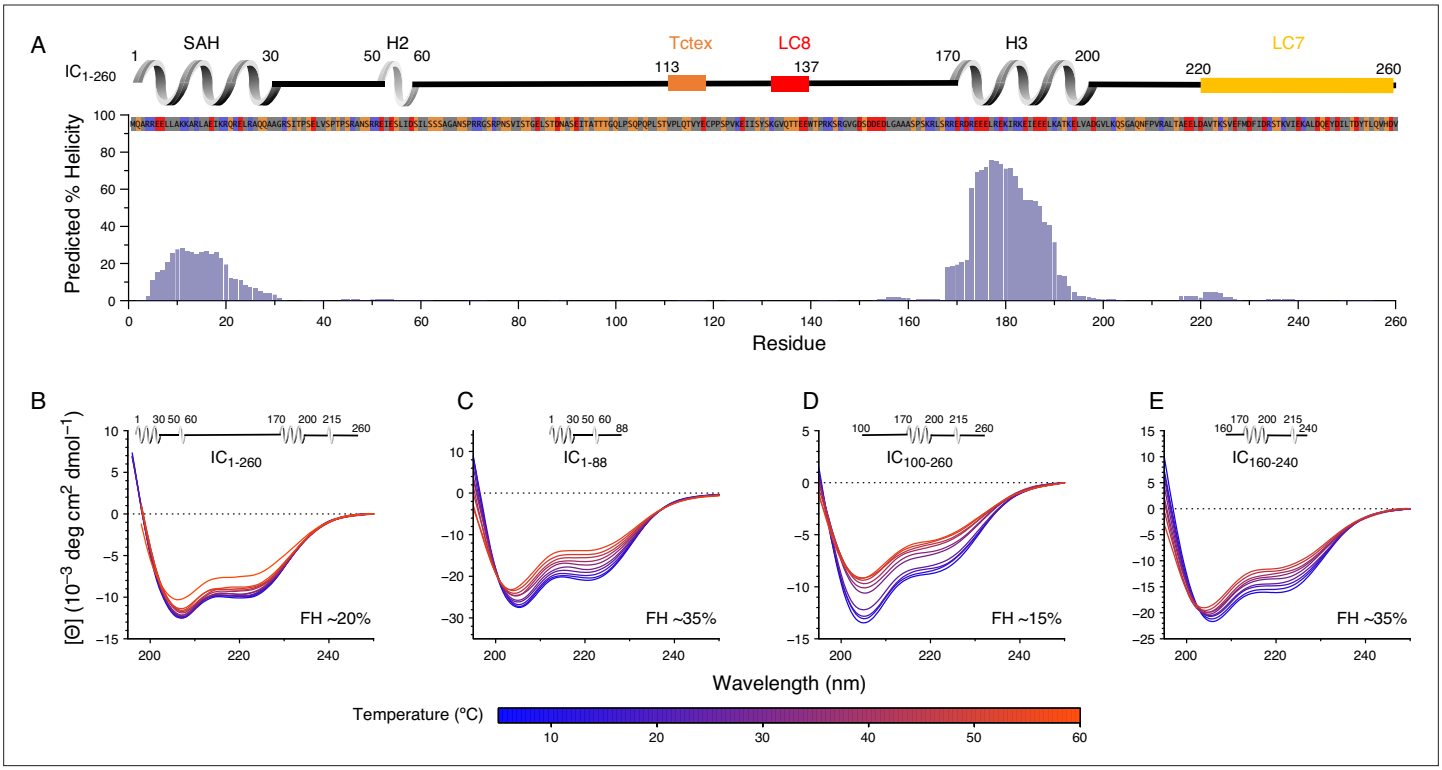

Figure 3. Secondary structure and thermal stability of *Chaetomium thermophilum* (Ct) intermediate chain (IC). (**A**) Agadir prediction for $IC_{1\text{-}260}$ showing the percent helicity by residue (purple). Shown above the plot is a schematic structure for $IC_{1\text{-}260}$ with labels for single α-helix (SAH), H2, and H3 above the helical structure. The sites for lights chain binding are also indicated. The amino acid sequence under the schematic is colored by amino acid type: hydrophobic (gray), positive (red), negative (blue), and neutral (orange). Variable temperature CD spectra of (**B**) $IC_{1\text{-}260}$, (**C**) $IC_{1\text{-}88}$, (**D**) $IC_{100\text{-}260}$, and (**E**) $IC_{160\text{-}240}$. The shapes of the spectra for all constructs indicate a mixture of α-helical secondary structure and regions of intrinsic disorder. Loss in structure, or lack thereof, over a temperature range of 5–50°C (blue for lowest, red for highest) indicates how each construct varies in stability and indicates that $IC_{1\text{-}260}$ is the most thermally stable. The fractional helicity (FH) of each construct at 5°C was calculated based on the experimentally observed mean residue ellipticity at 222 nm as explained in the Methods section.

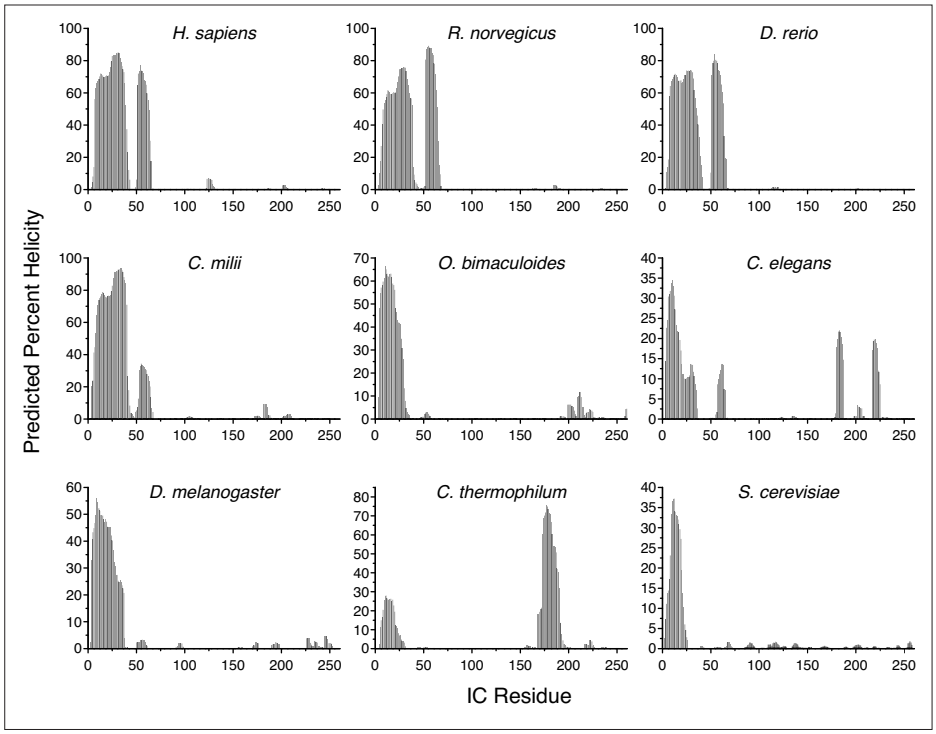

Figure 3—figure supplement 1. Predicted percent helicity in intermediate chain (IC) across species. Residue-level percent helicity predictions generated using the Agadir algorithm for the first 260 amino acids of IC from *Homo sapiens* (human), *Rattus norvegicus* (rat), *Danio rerio* (zebrafish), *Callorhinchus milii* (Australian ghostshark), *Octopus bimaculoides* (Californian two-spot octopus), *Caenorhabditis elegans* (nematode), *Drosophila melanogaster* (fruit fly), *Chaetomium thermophilum* (thermophilic fungus), and *Saccharomyces cerevisiae* (yeast) (***Muñoz and Serrano, 1997***; ***Muñoz and Serrano, 1994***; ***Muñoz and Serrano, 1995a***; ***Muñoz and Serrano, 1995b***).

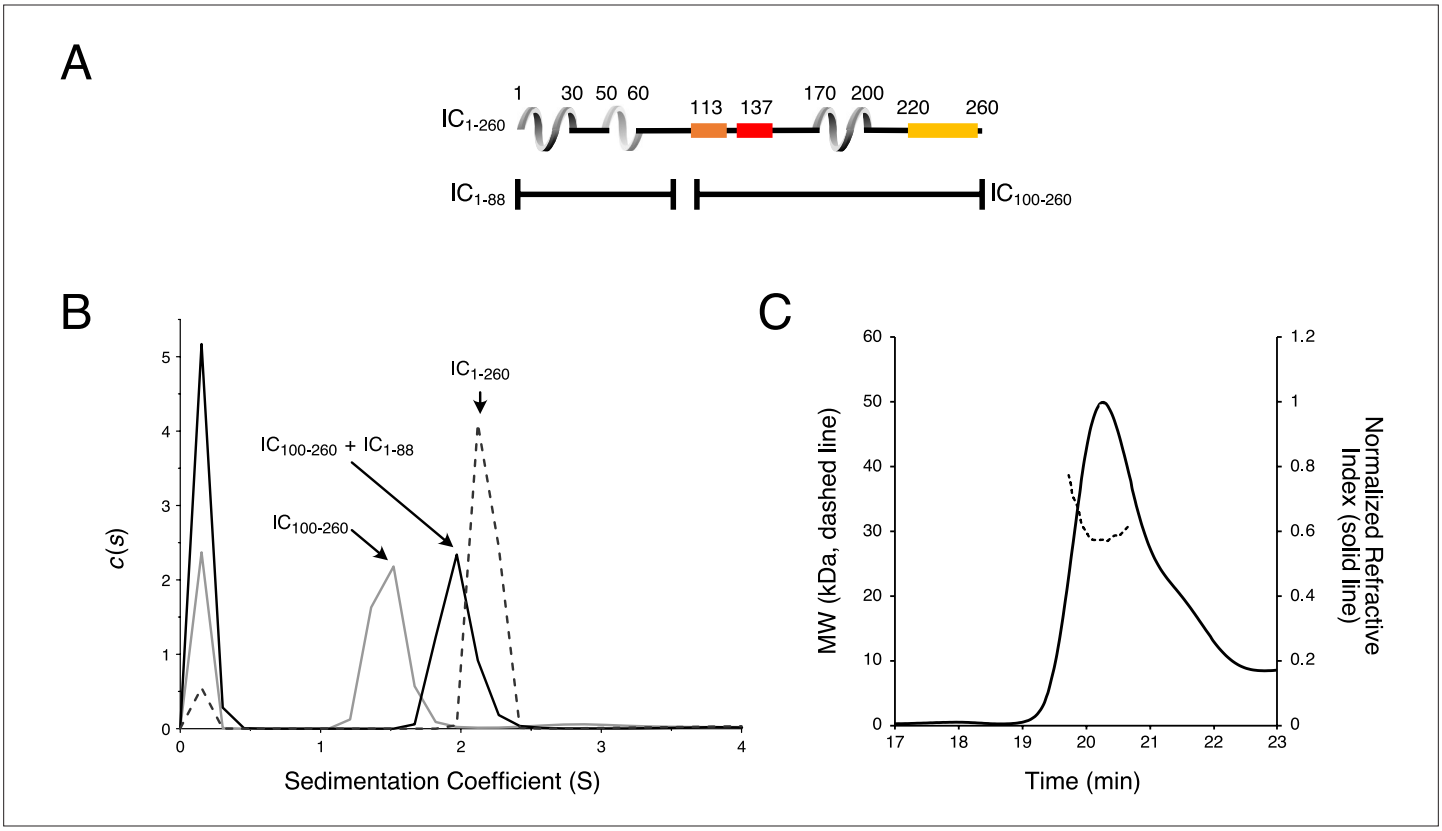

Figure 3—figure supplement 2. *Chaetomium thermophilum* (Ct) $IC_{1\text{-}88}$ and Ct $IC_{100\text{-}260}$ binding by sedimentation velocity analytical ultracentrifugation (SV-AUC). (**A**) Domain architecture diagrams of $IC_{1\text{-}260}$, $IC_{1\text{-}88}$, and $IC_{100\text{-}260}$. (**B**) SV-AUC experiments of $IC_{100\text{-}260}$ (gray), $IC_{100\text{-}260}$ mixed with $IC_{1\text{-}88}$ at a 1:2 molar ratio (black), and $IC_{1\text{-}260}$ (gray dashes). (**C**) The estimated mass of $IC_{100\text{-}260}$/$IC_{1\text{-}88}$ complex from MALS is 30.3 kDa, which indicates a 1:1 binding stoichiometry.

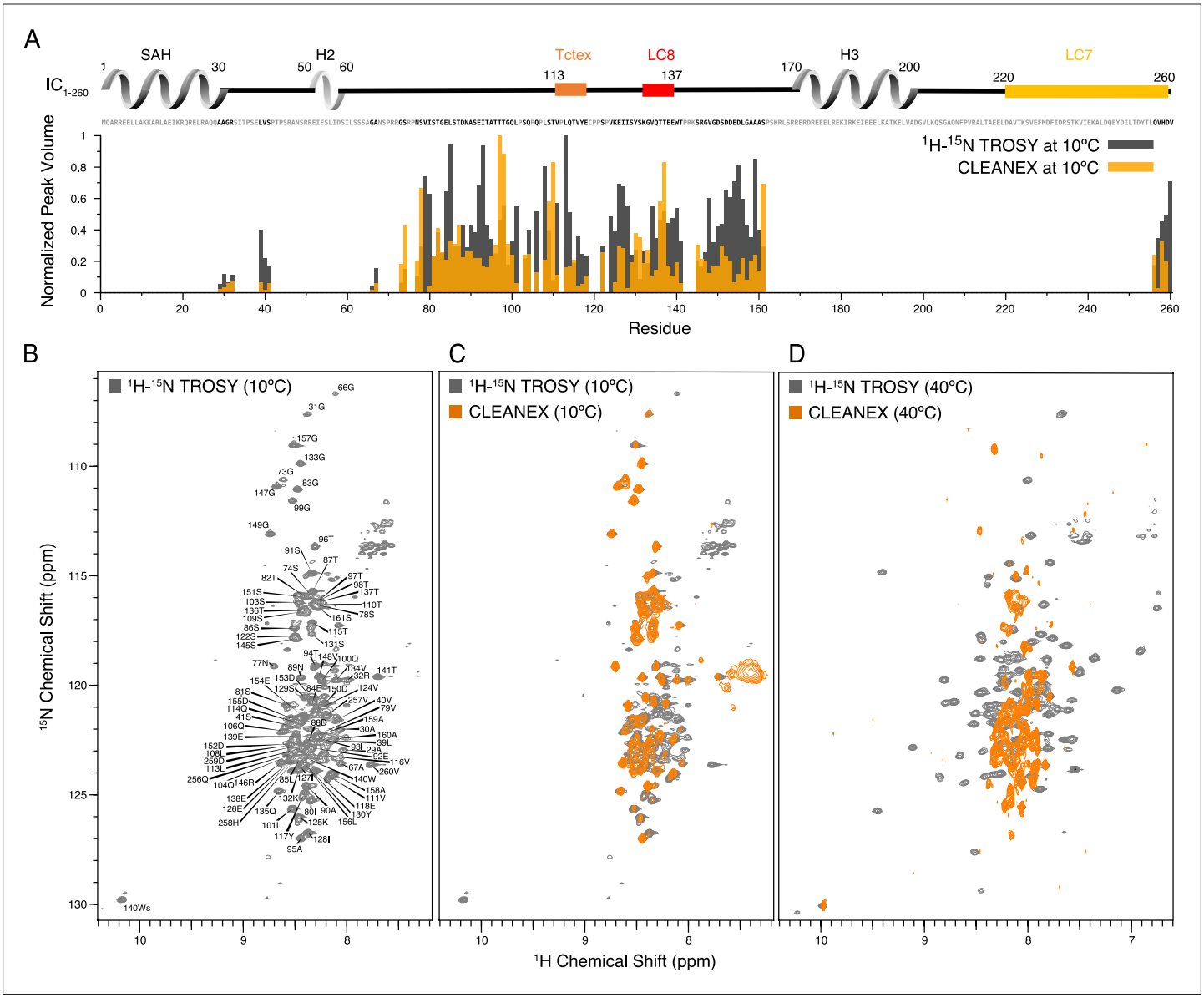

Figure 4. Identification of disordered linkers of *Chaetomium thermophilum* $IC_{1\text{-}260}$ using nuclear magnetic resonance spectroscopy. (**A**) Plot showing the normalized peak volumes at 10°C in the ^{1}H-^{15}N TROSY spectrum (gray) and in the CLEANEX spectrum (orange) of the amides that could be assigned. Assigned residues are in black in the sequence above the plot (and unassigned residues in gray); all assigned residues are from disordered regions of $IC_{1\text{-}260}$. (**B**) ^{1}H-^{15}N TROSY spectrum of $IC_{1\text{-}260}$ acquired at 800 MHz at 10°C showing amide assignments. (**C**) Overlay of a CLEANEX spectrum (orange) with the ^{1}H-^{15}N TROSY spectrum (gray) at 10°C, shows that most of the assignable residues are in exchange with the solvent on the timescale of the CLEANEX experiment. (**D**) At 40°C, ^{1}H-^{15}N TROSY spectrum (gray) shows new peaks appearing with greater chemical shift dispersion for $IC_{1\text{-}260}$ in the 800 MHz. Overlaying a CLEANEX spectrum (orange) at this temperature reveals that most of the new peaks in the ^{1}H-^{15}N TROSY spectrum are from amides that are slow to exchange with the solvent and therefore are not observed in the CLEANEX spectrum.

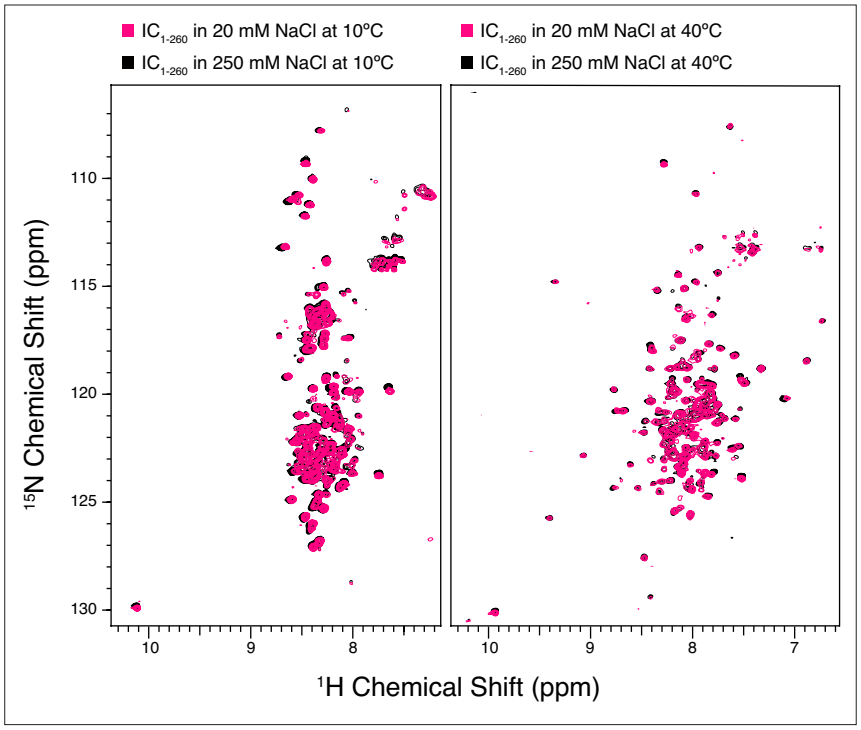

Figure 4—figure supplement 1. Nuclear magnetic resonance spectra of intermediate chain (IC) are unaffected by salt concentration. ^{1}H-^{15}N TROSY spectra of IC_{1-260} in 20 mM NaCl (black) overlaid with IC_{1-260} in 250 mM NaCl (pink) at both 10°C (left) and at 40°C (right).

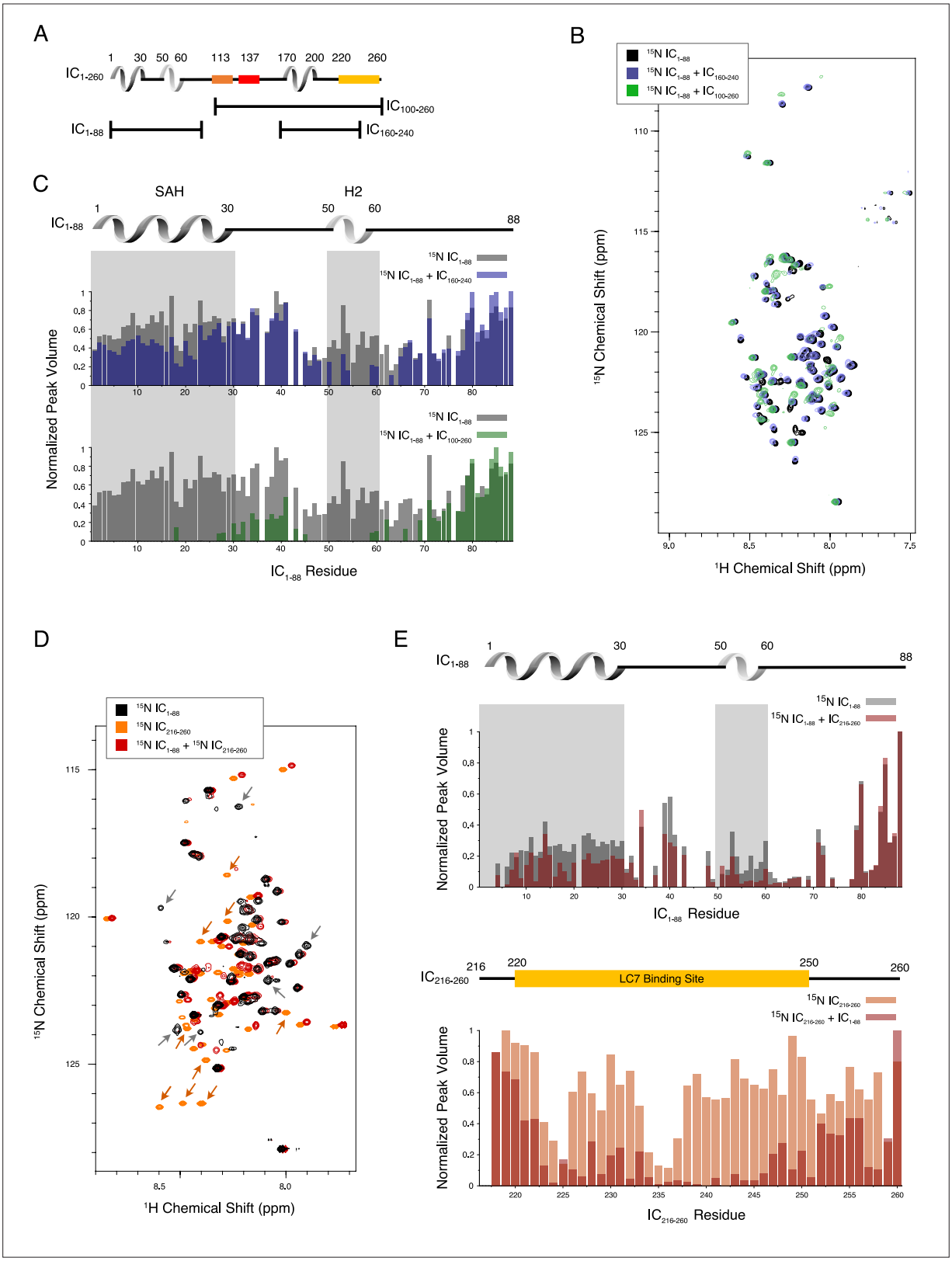

Figure 5. Evidence of tertiary contacts between the N and C-termini within *Chaetomium thermophilum* $IC_{1\text{-}260}$. (**A**) Domain architecture diagram for $IC_{1\text{-}260}$ with bars shown below corresponding to the $IC_{100\text{-}260}$, $IC_{1\text{-}88}$, and $IC_{160\text{-}240}$ constructs. (**B**) ^{1}H-^{15}N TROSY overlays of free ^{15}N-labeled $IC_{1\text{-}88}$ (black) and ^{15}N-labeled $IC_{1\text{-}260}$ bound to unlabeled $IC_{160\text{-}240}$ (purple) and $IC_{100\text{-}260}$ (green). Note, spectra are deliberately offset in the ^{1}H dimension to help visualize overlapping peaks. (**C**) Normalized peak volumes in the ^{1}H-^{15}N TROSY spectra for (top) ^{15}N-labeled $IC_{1\text{–}88}$ (gray) and ^{15}N-labeled $IC_{1\text{–}88}$ + $IC_{160\text{-}240}$ (purple)

Figure 5 continued on next page

Figure 5 continued

and (bottom) ^{15}N-labeled $IC_{1–88}$ (gray) and ^{15}N-labeled $IC_{1–88}$ + $IC_{100-260}$ (green). (**D**) ^{1}H-^{15}N HSQC overlay of ^{15}N-labeled IC_{1-88} (black), ^{15}N-labeled $IC_{216-260}$ (orange), and ^{15}N-labeled $IC_{216-260}$ bound to ^{15}N-labeled IC_{1-88} (red). Arrows highlight some of the more significant peak disappearances for IC_{1-88} (gray arrows) and $IC_{216-260}$ (orange arrows). Note, spectra are deliberately offset by 0.03 ppm in the ^{1}H dimension to help visualize overlapping peaks. (**E**) Normalized peak volumes in the ^{1}H-^{15}N HSQC spectra for ^{15}N-labeled $IC_{216-260}$ (top, gray columns) and ^{15}N-labeled $IC_{216-260}$ (bottom, orange columns) when free and when in the presence of the other protein (red columns).

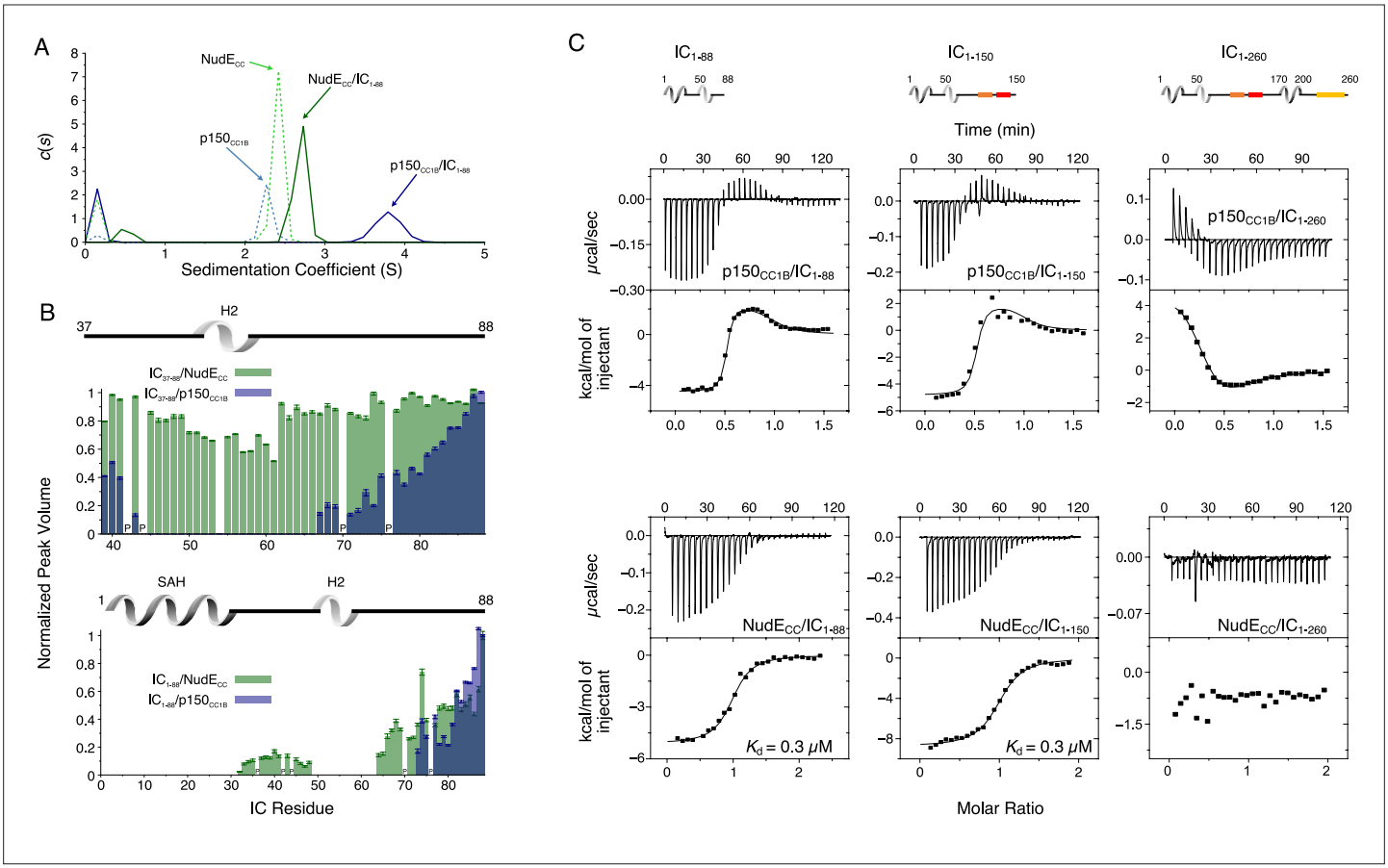

Figure 6. Binding interactions of *Chaetomium thermophilum* intermediate chain (IC) to p150$_{CC1B}$ and NudE$_{CC}$. (**A**) Sedimentation velocity analytical ultracentrifugation profiles for samples containing p150$_{CC1B}$ (blue dashed line), NudE$_{CC}$ (green dashed line), IC$_{1-88}$/p150$_{CC1B}$ complex (blue solid line), and IC$_{1-88}$/NudE$_{CC}$ complex (green solid line) show that IC$_{1-88}$ complexes have a larger sedimentation coefficient with p150$_{CC1B}$ than with NudE$_{CC}$. No data were collected for free IC$_{1-88}$ because it has no absorbance at 280 nm. (**B**) Normalized peak volumes in the ^{1}H-^{15}N HSQC spectra for ^{15}N-labeled IC$_{37–88}$ (top) or ^{15}N-labeled IC$_{1–88}$ (bottom) when titrated with unlabeled p150$_{CC1B}$ (blue) and NudE$_{CC}$ (green). 'P' indicates proline residues. No peak disappearance for IC$_{37-88}$ was observed when NudE$_{CC}$ was added. Error bars are based on propagating the root-mean-square noise of the individual spectra. (**C**) Isothermal titration calorimetry (ITC) thermograms for p150$_{CC1B}$ titrated with IC$_{1-88}$ (top left), IC$_{1-150}$ (top middle), and IC$_{1-260}$ (top right), and for NudE$_{CC}$ titrated with IC$_{1-88}$ (bottom left), IC$_{1-150}$ (bottom middle), and IC$_{1-260}$ (bottom right), collected at 25°C (pH 7.5). Solid lines show fits to either a two-step binding model (p150$_{CC1B}$) or a one-site binding model (NudE$_{CC}$). For IC$_{1-260}$, reduced and endothermic binding is observed with p150$_{CC1B}$ whereas no binding is observed with NudE$_{CC}$.

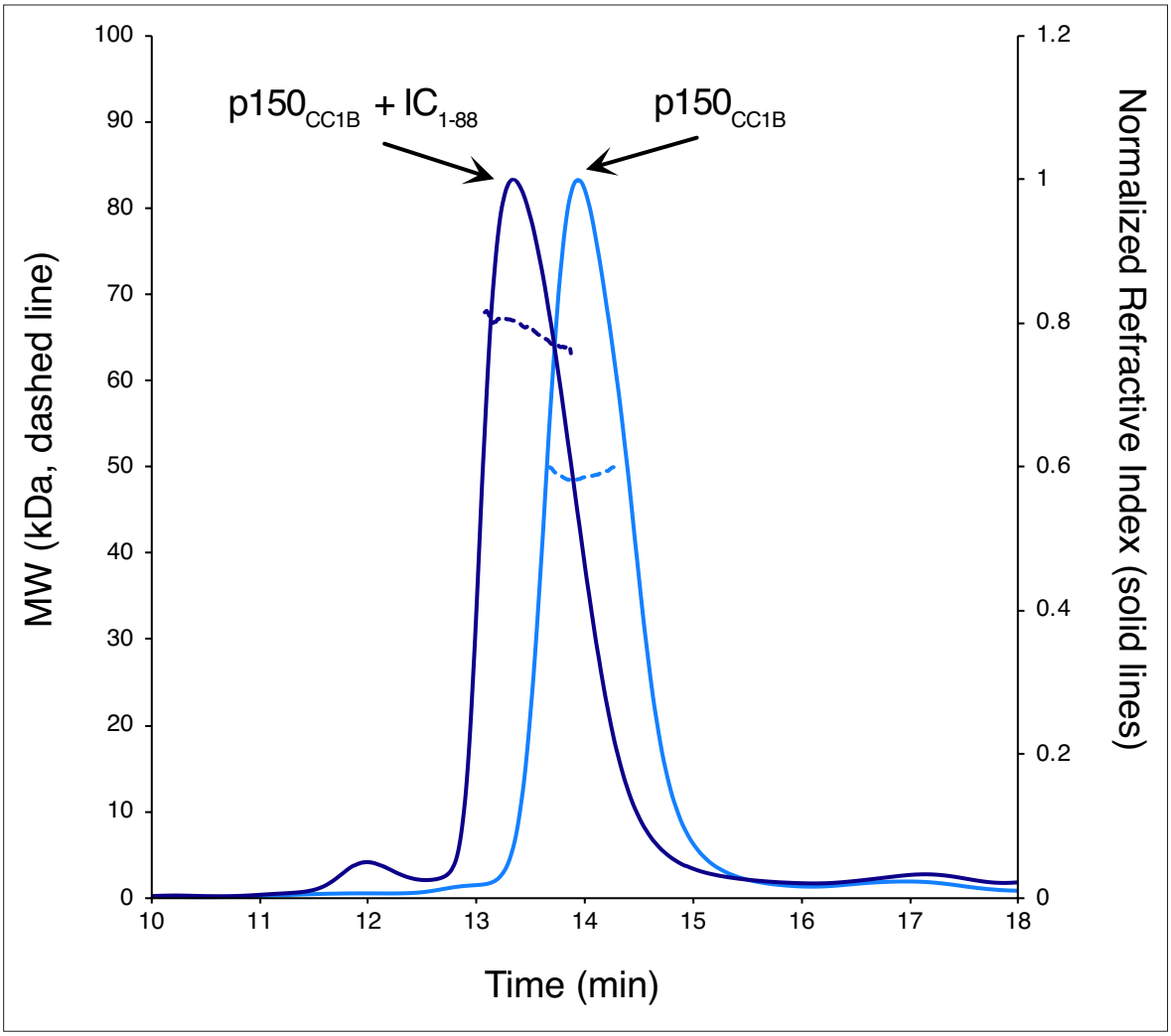

Figure 6—figure supplement 1. Size exclusion chromatography with multi-angle light scattering (SEC-MALS) of IC_{1-88} and $p150_{CC1B}$. The estimated mass of $p150_{CC1B}$ from MALS is 49 kDa (light blue) while the addition of IC_{1-88} increases the mass to 66 kDa (dark blue) indicating a complex containing a $p150_{CC1B}$ dimer and two IC_{1-88} chains.

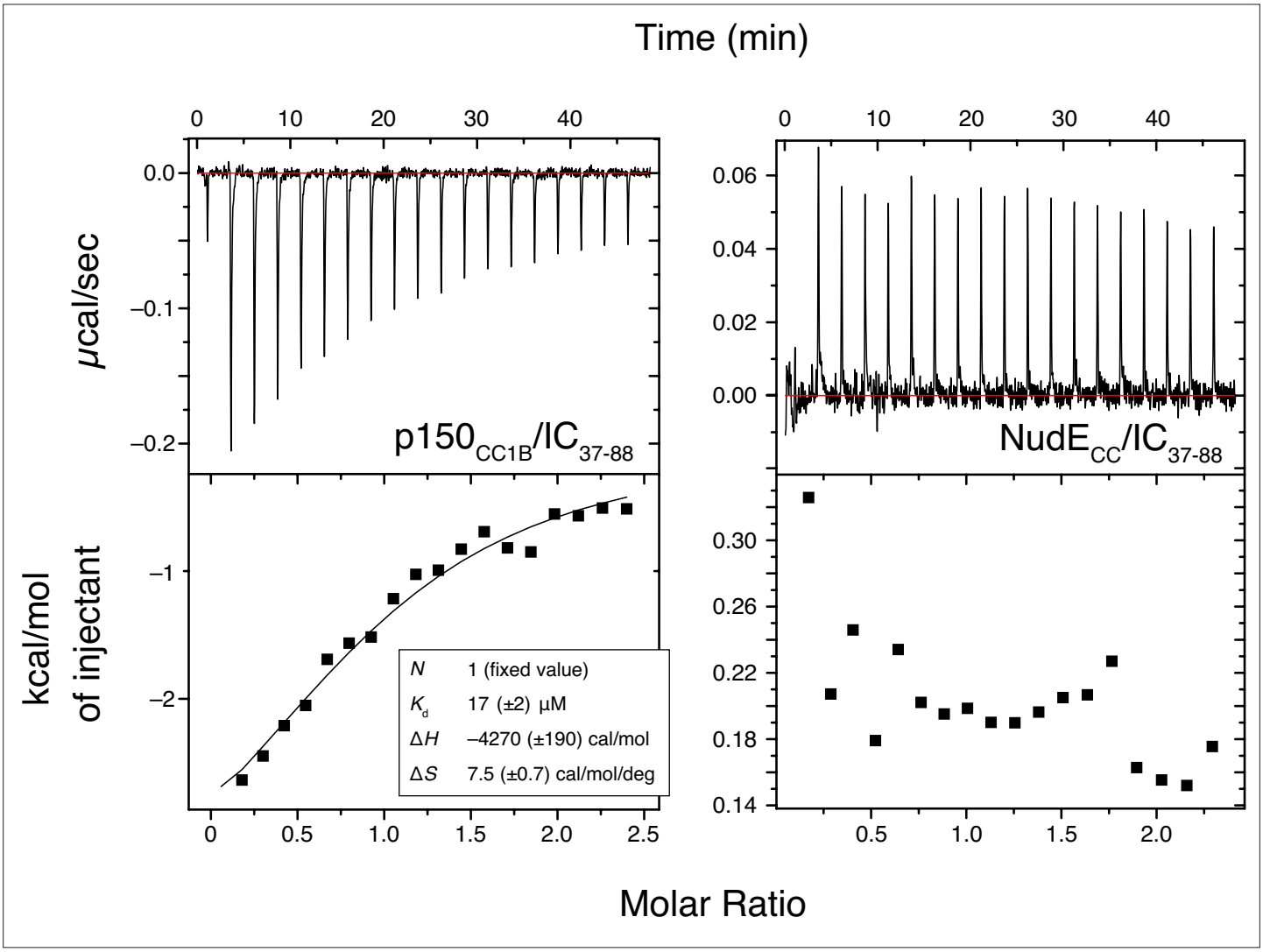

Figure 6—figure supplement 2. Binding interactions of *Chaetomium thermophilum* IC_{37-88} to $p150_{CC1B}$ and $NudE_{CC}$. ITC thermograms for $p150_{CC1B}$ titrated with IC_{37-88} (left) and $NudE_{CC}$ titrated with IC_{37-88} (right), collected at 25°C (pH 7.5). IC_{37-88} contains the H2 region of intermediate chain (IC) and binds weakly (K_d ~20 µM) to $p150_{CC1B}$ while no binding is detected for $NudE_{CC}$.

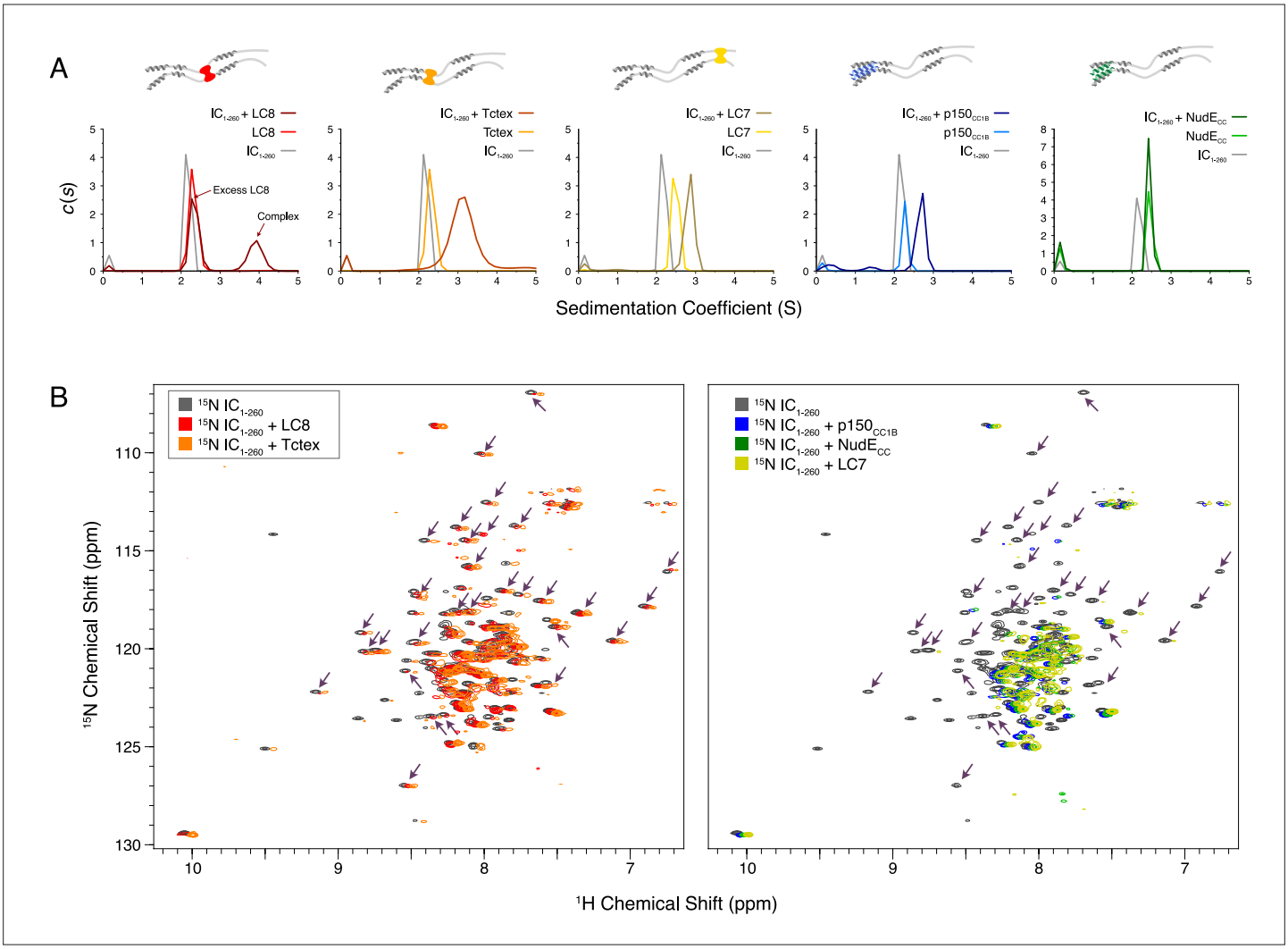

Figure 7. Binding characterization of binary complexes of IC_{1-260}. (**A**) Sedimentation velocity analytical ultracentrifugation of IC_{1-260}/LC8, IC_{1-260}/Tctex, IC_{1-260}/LC7, IC_{1-260}/$p150_{CC1B}$, and IC_{1-260}/$NudE_{CC}$. Data for the binary complexes is overlayed with data for each protein individually to better see shifts in the sedimentation coefficient of the binary complexes. (**B**) ^{1}H-^{15}N TROSY overlays of free ^{15}N-labeled IC_{1-260} (black) and ^{15}N-labeled IC_{1-260} bound to unlabeled binding partners in a 1:1.5 molar ratio. The spectra were offset by 0.03 ppm in the ^{1}H dimension to help illustrate changes in peak intensities. Changes in peak appearances/shifts/disappearances seem to be similar for LC8 (red) and Tctex (orange) versus changes seen for $p150_{CC1B}$ (blue), $NudE_{CC}$ (green), and LC7 (yellow). Arrows indicate peaks that remain when LC8 and Tctex are added to IC_{1-260}, but disappear when $p150_{CC1B}$, $NudE_{CC}$, and LC7 are added.

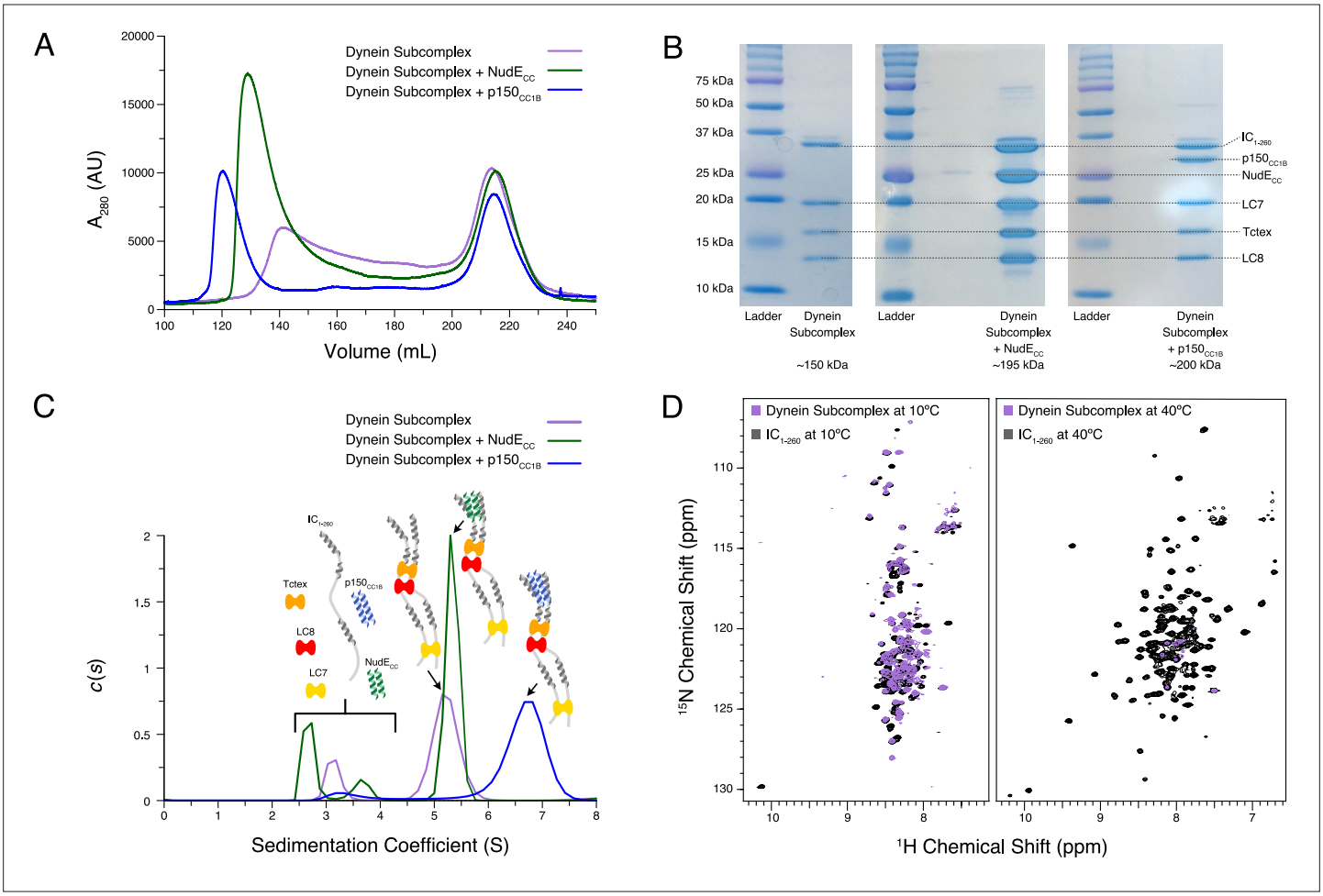

Figure 8. Reconstitution and characterization of dynein subcomplexes. (**A**) Size exclusion chromatography (SEC) traces of the dynein subcomplex (IC/light chains) (purple) and the dynein subcomplex with the addition of either p150$_{CC1B}$ (blue) or NudE$_{CC}$ (green). (**B**) Sodium dodecyl sulphate–polyacrylamide gel electrophoresis gels of fractions collected from SEC for all complexes showing all expected proteins. (**C**) SV-AUC profiles of the dynein subcomplex (purple) bound to p150$_{CC1B}$ (blue) or NudE$_{CC}$ (green). (**D**) ^{1}H-^{15}N TROSY overlays of free IC$_{1-260}$ (black) and the dynein subcomplex (purple). At 10°C, many peaks are still of high intensity in the 153 kDa complex, indicating that some regions remain disordered. The very few peaks at 40°C of the bound are most likely due to the size and tumbling of the subcomplex and consistent with the fact that the majority of the peaks at this temperature are from ordered regions.

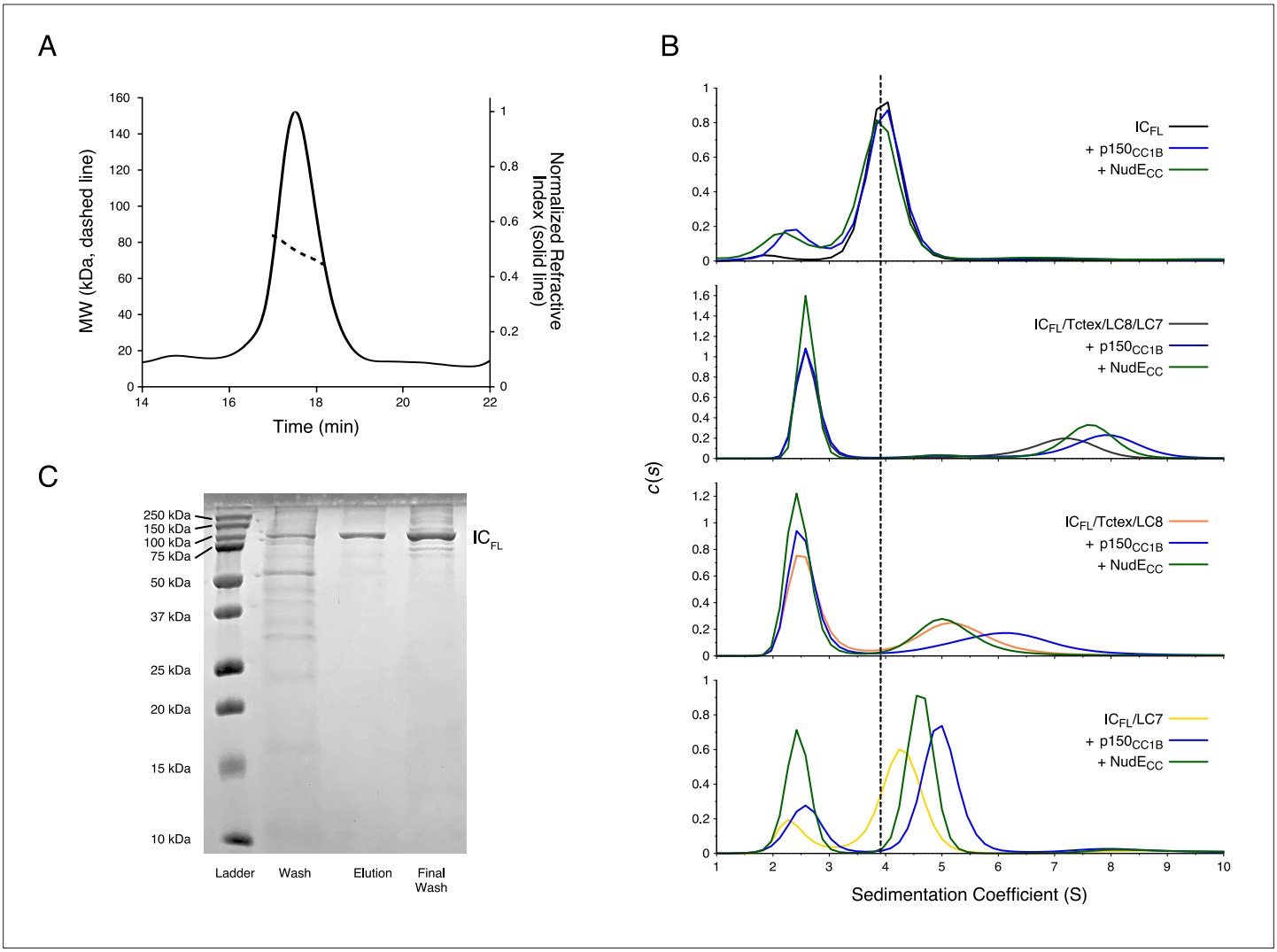

Figure 9. Binding characterization of *Chaetomium thermophilum* IC_{FL} subcomplexes. (**A**) The estimated mass of IC_{FL} from multi-angle light scattering is 75.4 kDa, which indicates that IC_{FL} is a monomer in the absence of binding partners. (**B**) Sedimentation velocity analytical ultracentrifugation profiles of IC_{FL} (black), IC_{FL} mixed with $p150_{CC1B}$ (blue) or $NudE_{CC}$ (green), and the subcomplexes: IC_{FL}/Tctex/LC8/LC7 (gray), IC_{FL}/Tctex/LC8/LC7/$p150_{CC1B}$ (blue), IC_{FL}/Tctex/LC8/LC7/$NudE_{CC}$ (green), IC_{FL}/Tctex/LC8 (orange), IC_{FL}/Tctex/LC8/$p150_{CC1B}$ (blue), IC_{FL}/Tctex/LC8/$NudE_{CC}$ (green), IC_{FL}/LC7 (yellow), IC_{FL}/LC7/$p150_{CC1B}$ (blue), and IC_{FL}/LC7/$NudE_{CC}$ (green). The black, dashed line is centered on unbound IC_{FL} to help guide the eye. (**C**) Sodium dodecyl sulphate–polyacrylamide gel electrophoresis gel of immobilized metal affinity chromatography fractions (left to right: wash, elution, and final wash) with a band for IC_{FL} migrating in accordance with the expected mass of ~79 kDa.

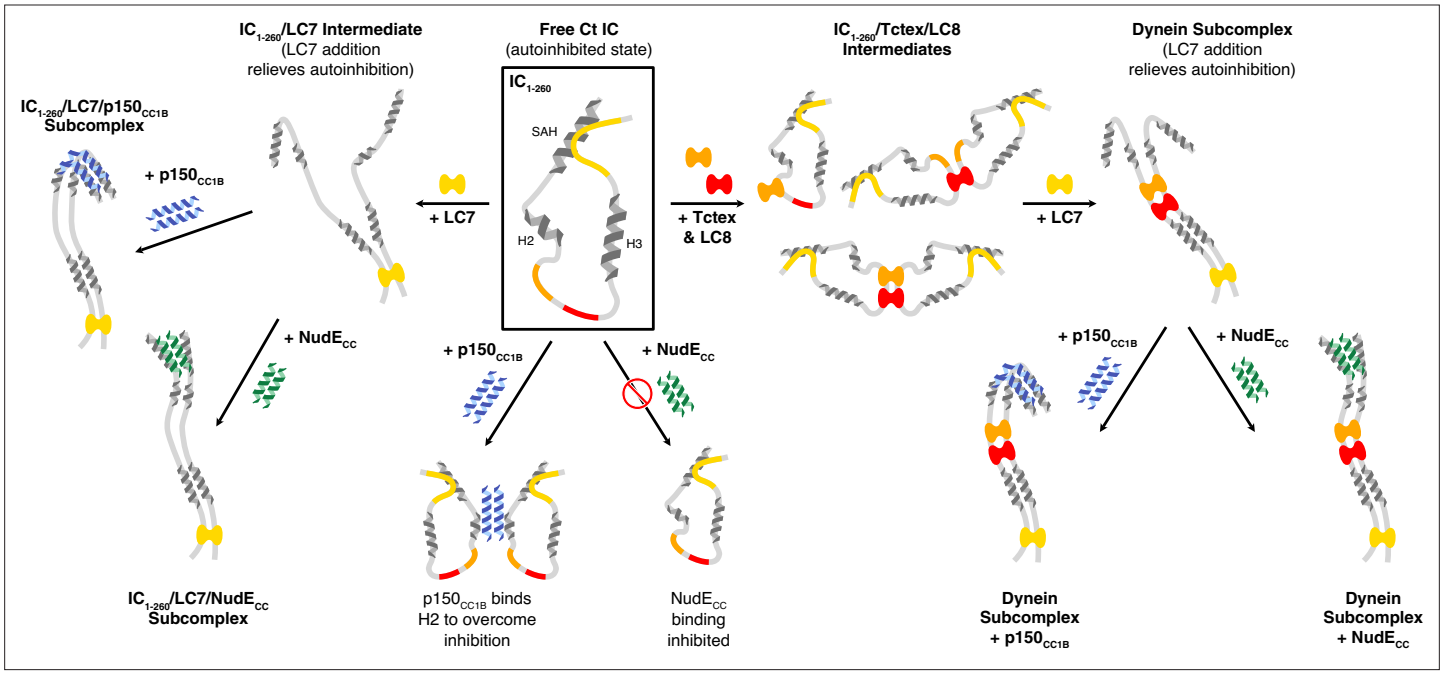

Figure 10. A model of *Chaetomium thermophilum* $IC_{1\text{-}260}$ binding interactions and subcomplex assemblies. Free $IC_{1\text{-}260}$ is compact and in autoinhibited state (Boxed in black), with the single α-helix (SAH), H2, and H3 regions depicted as helices and with colors indicating the LC8 (red), Tctex (orange), and LC7 (yellow) binding sites. When LC7 is added (left arrow) LC7 outcompetes autoinhibition to bind $IC_{1\text{-}260}$, exposing the SAH domain for $p150_{CC1B}$ and NudE binding. When $p150_{CC1B}$ or $NudE_{CC}$ is added (down arrows) to free $IC_{1\text{-}260}$, autoinhibition prevents $NudE_{CC}$ from binding and reduces the binding affinity of $p150_{CC1B}$. However, as $p150_{CC1B}$ is able to bind to the H2 region of $IC_{1\text{-}260}$, binding is not completely prevented. Addition of Tctex and/or LC8 (right arrow) leads to a number of possible binary and ternary intermediates. LC8's role of driving IC dimerization is depicted and, in all intermediates, we predict that IC autoinhibition remains based on very limited changes in nuclear magnetic resonance spectra. Continuing to the right, the addition of LC7 leads to formation of the dynein subcomplex and the release of SAH autoinhibition. The free SAH is now able to resume transient interactions with H2 prior to binding with either $p150_{CC1B}$ or $NudE_{CC}$. Finally, addition of $p150_{CC1B}$ or $NudE_{CC}$ leads to the formation of the p150 and NudE subcomplexes (bottom right). Our sedimentation velocity analytical ultracentrifugation data suggest that the NudE subcomplex adopts a more elongated conformation.